Supporting Material for **"Single molecule characterization of α-Synuclein in aggregation-prone states"**

Adam J. Trexler and Elizabeth Rhoades

Labeling

The initial conditions for labeling were 100 μM αS in a total volume of 200 μL buffer (20 mM Tris pH 7.4, 50 mM NaCl). Reactions were performed in the dark at room temperature. We employed a sequential labeling scheme whereby αS was first incubated with ~2X (molar ratio) acceptor dye (Alexa Fluor 594 maleimide; Invitrogen) for 25 minutes, followed by removal of unconjugated acceptor fluorophore with two stacked 5 mL GE HiTrap desalting columns. This sample was then run over an anion exchange column (5 mL GE HiTrap FF) which partially removes unlabeled proteins. The protein was then incubated with ~1X donor dye for 3 minutes (Alexa Fluor 488 maleimide; Invitrogen) followed by another passage over the desalting columns to remove unconjugated donor fluorophore.

Our labeling method is designed to minimize the number of donor-only labeled protein (either by having only a donor present at a single position or a donor present at both positions), as these are a major component of the artifactual ET_{eff}~0 (zero-peak) commonly observed in diffusion-based smFRET measurements. In the first step, we expect that many proteins may be labeled with two acceptor fluorophores, but these are essentially invisible in our measurements as the acceptor fluorophore is not directly excited. Molecules with a single acceptor are available in the second step for donor labeling. A small amount of donor in the second labeling reaction is utilized in order to minimize the possibility of labeling any remaining unlabeled protein with two donor fluorophores. Our method uses identical chemistry (cysteine residues with maleimide fluorophores) for both labeling sites, thus we cannot control at which cysteine (position X or Y) the donor or acceptor label is attached. If the donor or acceptor is differentially quenched or rotationally constrained at position X or Y, it may result in artifacts in the ET_{eff} histograms (shifts in the peak positions, appearance of multiple peaks). However, we expect a different distribution of fluorophores at each labeling site for each labeling reaction and have not observed any evidence of shifts in the position of the ET_{eff} histogram peaks, dramatic changes in histogram widths, or the presence of subpopulations between different labeling reactions. Furthermore, we have performed anisotropy and lifetime measurements of each fluorophore at all labeling sites used in this study (below). These measurements show that the fluorophores are not differentially constrained or quenched at any particular position with αS, indicating that in terms of our FRET measurements, these fluorophores behave very similarly regardless of whether they are at position X or Y in a given double mutant. Based on the reproducibility of the ET_{eff} measurements, along with anisotropy and lifetime measurements, we are confident that site-specific labeling artifacts are not contributing to our ET_{eff} measurements.

As seen below in Figure S1, in some of our labeling reactions the zero-peak is not insignificant. While a large portion of this may be due to inefficient labeling reactions (the generation of donor-only or double-donor labeled proteins), we believe a fraction may be due to photophysical effects, such as photodamage to the acceptor fluorophore

(1). We are currently developing methods for limiting this effect: primarily by removing oxygen from our experimental system and developing better methods for fluorophore handling prior to labeling.

Instrumentation

Our instrument is a home-built system based on an Olympus IX-71 inverted microscope and a 488 nm DPSS laser, previously described and similar to other setups described in the literature (2, 3). Laser power was 15-25 μW, measured directly before entering the microscope. Fluorescence emission was collected through the objective, and donor and acceptor photons were separated by a HQ585LP dichroic mirror (Chroma, Bellows Falls, VT), and then further selected using band-pass filters: ET 525/50M for the donor, HQ600LP for the acceptor (Chroma). The fluorescence was collected by fiber-coupled avalanche photodiodes (100 μm diameter) connected to a hardware correlator (Correlator.com, Bridgewater, NJ). Photon traces were usually collected in 1 ms time bins.

ET_{eff} is calculated by $ET_{eff}= (I_a- \beta*I_d) / (I_a + \gamma*I_d)$. β and γ are correction factors which we have experimentally measured for our system. β accounts for donor fluorescence bleed-through to the acceptor channel (0.06 for Alexa Fluor 488 in our system with the filters described above). γ accounts for differences in detection efficiency and quantum yield for the fluorophores and is given by, $\gamma= \varphi A*\eta A/\varphi D*\eta D$, where φA and φD are the quantum yields of the acceptor and donor fluorophores, and ηA and ηD are the detection efficiencies of the acceptor and donor fluorophores. There are a variety of methods for empirically calculating γ, but we have chosen to compare the fluorescence intensity of the donor and acceptor fluorophores between a detector-calibrated fluorometer and our instrument (4). For our system with Alexa Fluor 488 and Alexa Fluor 594 as donor and acceptor, respectively, γ=1.2. Our setup and correction factors have been experimentally validated by the measurement of polyproline peptides, which have been commonly used in the literature as distance standards (4). We have previously reported that ET_{eff} values of polyproline 6 and polyproline 20 measured on our system are in good agreement with the literature (2).

Burst Selection and Data Analysis

To select bursts arising from protein transits through the focal volume, we used three criteria: (1) the sum of the photons detected by the donor and acceptor channels was greater than the experimentally determined donor cut-off (described below); (2) the acceptor channel counts were greater than the experimentally determined acceptor cut-off; and (3) the donor channel counts were greater than zero. Cut-off values were determined by comparing photon traces of buffer in the absence and presence of protein. These photon traces are histogrammed according to the number of photons per 1 ms time bin. A signal to noise ratio for each photon value is calculated by dividing each time bin from protein histogram value by the corresponding time bin from the buffer histogram. For example, for a bin corresponding to 10 photons detected, the protein bin may have 100 events, whereas the buffer bin has 5 events, and their ratio is 100/5=20. The number of photons that results in the highest ratio is chosen as the cut-off.

The sum cut-off allows for discrimination between photons due to protein transit from photons due to background. The second two criteria allow us to eliminate artifactual events at 0 and 1 $ET_{eff.}$ These events are well known in smFRET measurements and arise from molecules that have either been incompletely labeled (in most cases due to an absent acceptor fluorophore) or from molecules where the fluorophores are present, but inactive due to photobleaching or other effects. The sum cut-off was typically ~25 photons, and the acceptor cut-off ~10 photons, usually changing by a few photons between measurements as a function of the particular laser power used for individual measurements. These criteria routinely identify zero events in photon traces of buffer alone, showing that they effectively discriminate background signal from protein.

The first concern when applying an acceptor cut-off to eliminate the zero-peak is whether the position and shape of the ET_{eff} histogram are affected. While the sum cut-off modifies the total number of events that are assigned to protein transit, the acceptor cut-off must be used cautiously as increasing this value can lead to artifactual shifts of the ET_{eff} peak, by discriminating against legitimate protein events with a low ET_{eff} values (i.e. with fewer photons in the acceptor channel). We took care to use a minimal acceptor cut-off to eliminate zero-peak events while not shifting the position of the ET_{eff} peak by analyzing our data with progressive acceptor cut-offs, as shown in Figure S1. We have shown previously (2), and illustrate in Figure S1C, that use of an appropriate acceptor cut-off for ET_{eff} peaks >0.50 does not lead to significant shifts of the peak. We show in Figure S1A-B that applying an appropriate acceptor cut-off to our αS constructs with the lowest ET_{eff} values (9-130 and 33-130 at pH 7.4) does not perturb the position of the ET_{eff} peak. In the case of 9-130 construct, a small shift is observed (x_c=0.35 to x_c=0.39) when applying an acceptor cut-off of 11, which emphasizes the importance of caution when analyzing this region of the ET_{eff} histogram. However, given the small size of this shift, and the fact that the pH 7.4 and pH 3.0 histograms for this construct have been treated with very similar cut-offs, we are confident in the conclusion (discussed below) there is no significant shift between the two pH conditions for this mutant. The exact position of the ET_{eff} peak is difficult to ascertain, but this value is not vital to the conclusions we draw.

The second concern is whether there are low ET_{eff} populations present that the zero-peak obscures our ability to detect or that are inappropriately eliminated by use of the acceptor cutoff. For illustration purposes, consider a case where two populations (stable on the ~1ms timescale of the ET_{eff} measurement; as discussed in the manuscript, very fast interchange between populations is not resolvable in our measurements and thus must be considered a single population) are present. For constructs where the probes are placed relatively close together, the ET_{eff} of both populations would be high enough that two peaks should be seen in the distribution, even if the second population were very extended. We see no evidence of this in our shorter distance constructs (for instance, constructs 72-92, 54-72, or 92-130). For constructs where longer distances are probed (such as the 9-130 construct), we cannot state with complete certainty that there are not two states, one of which is obscured by the zero-peak. Such a scenario, however, seems unlikely, given that single populations are observed for all constructs with more closely spaced probes. Further evidence in support of a single population of αS in solution comes

from a study using alternating laser excitation (ALEX), which allows for direct excitation of the acceptor fluorophore and thus the discrimination of low ET_{eff} events from zero-peak events, that also did not find any evidence of very low ET_{eff} populations of αS in solution (5).

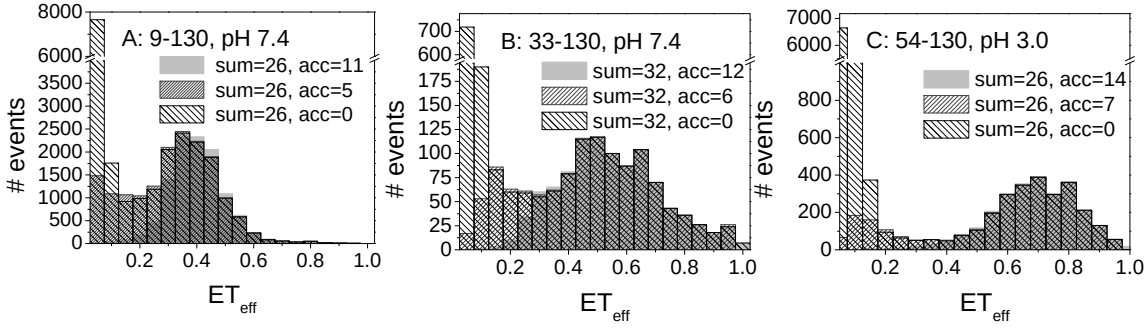

Figure S1. Acceptor cut-offs do not shift ET_{eff} distributions. In each panel, the sum cut-off is held constant while the acceptor cut-off is increased from 0 to the acceptor threshold value used for analysis. Three different constructs with different peak ET_{eff} values are shown, in order to illustrate the effect of this analysis approach as a function of mean $ET_{eff.}$ In B-C there is virtually no perturbation of the peak at ET_{eff}~ 0.5 and 0.75, respectively, and the zero peak is effectively eliminated. In panel A, with peak at ET_{eff}~0.35, a small shift, <0.05 ET_{eff}, is observable.

Anisotropy

Steady state fluorescence anisotropy measurements were made at a variety of labeling positions to ensure that fluorophore rotation was not significantly hindered by interactions with the protein. Given that random fluorescent dipole orientation is a key assumption in FRET, we wanted to ensure that no one position in αS restricted fluorophore motion than any other. We previously measured Alexa Fluor 488 and Alexa Fluor 594 at positions 9, 33, and 72 and found similar rotation for these fluorophores at each position (2). For the current study, we measured positions 9, 33, 54, 72, 92, and 130 at both pH 7.4 and pH 3.0. A PTI ISS fluorometer was used for all measurements, and fluorescence emission intensity was collected for 60 seconds and the average value was used for calculations. The G factor was calculated by measuring free Alexa Fluor 488 or Alexa Fluor 594 dye by $G= I_{hv}/I_{hh}$. Fluorescence intensity was measured for 20-50 nM αS in 20mM Tris 50mM NaCl pH 7.4 or pH 3.0. Anisotropy (r) was calculated as $r= I_{vv} – G*I_{vh} / I_{vv}+ 2*G*I_{vh}$. Anisotropy values are listed in Table S1. We observed that Alexa Fluor 488 had a lower average anisotropy than Alexa Fluor 594, which is expected given the larger size and increased hydrophobicity of Alexa Fluor 594. We also observed small increases in anisotropy for both dyes at pH 3.0, which we also expect given the compaction and likely rigidification of αS at low pH. All anisotropy values were < 0.15, which indicates that rotational constraint should not introduce significant artifacts into our FRET measurements (6, 7).

Fluorescence lifetime measurements

Fluorescence lifetime measurements were performed on a Fluorolog TCSPC fluorometer (Horiba Jobin Yvon, Edison, NJ). A 459nm NanoLED and 566nm NanoLED were used to excite Alexa Fluor 488 and Alexa Fluor 594, respectively. Each day an instrument response decay was collected for each NanoLED using a scattering solution (LUDOX LS colloidal silica). 2μM αS labeled with either Alexa Fluor 488 or Alexa Fluor 594 was then measured until 10,000 events were detected, and the distribution of lifetimes from this measurement was fit using one or two exponential decays. Values are listed in Table S1.

Position	pH	A488 Anisotropy (AU)	A488 Lifetime (ns)	A594 Anisotropy (AU)	A594 Lifetime (ns)
S9	7.4	0.066	3.9 (94%), 1.9(5.9%)	0.137	4.4
	3.0	0.096	3.9 (93%), 2.1 (7%)	0.128	4.4
T33	7.4	0.09	3.9 (94%), 1.6 (6%)	0.123	4.4
	3.0	0.067	4 (96%), 1.5 (4%)	0.154	4.4
T54	7.4	0.074	4 (93%), 2.5 (7%)	0.12	4.4
	3.0	0.076	4 (93%), 2.5 (7%)	0.161	4.4
T72	7.4	0.059	4.2	0.119	4.4
	3.0	0.094	4.1	0.131	4.3
T92	7.4	0.035	4.2 (96%), 7.6 (4%)	0.096	4.4
	3.0	0.046	4.2	0.075	4.4
E130	7.4	0.078	3.3 (91%), 1.4 (9%)	0.111	4.4
	3.0	0.109	3.4 (89%), 1.6 (11%)	0.156	4.4

Table S1. Fluorescence parameters for singly labeled αS constructs. Anisotropies and lifetimes are given for both Alexa Fluor 488 (A488) and Alexa Fluor 594 (A594) attached to single cysteine αS constructs. Single cysteine constructs were made for each labeling site used for smFRET constructs.

Fluorescence correlation spectroscopy (FCS) measurements

FCS measurements were performed on the same instrument used for smFRET measurements and in the same treated chambered coverglasses as described in the text. The laser power was set to 5 μW. αS was labeled at position 130 with Alexa Fluor 488 maleimide, based on the manufacturer's instructions (Invitrogen). Labeled αS was diluted to 50 nM into 20 mM Tris pH 7.4 or 3.0, 140 mM NaCl. Fifty 10-second measurements were made, and the data was analyzed in subsets of five to determine the average diffusion time of the protein for both conditions. Analysis was performed as previously described (8, 9). Autocorrelation curves were generated by a hardware correlator (Correlator.com) and fit using the standard equation (Eq .1) for a single species diffusing in 3 dimensions in a diffraction limited observation volume:

Eq 1: $$G(\tau) = \frac{1}{N}\left[1+\frac{\tau}{\tau_D}\right]^{-1}\left[1+\frac{\tau}{\omega^2\tau_D}\right]^{-\frac{1}{2}}$$

where N is the average number of particles in the focal volume, τ_D is the diffusion time of the protein, and ω is the structure factor which relates to the axial to radial dimensions of the focal volume. All ten subsets were then used to calculate a total average diffusion time in pH 7.4 and 3.0. These averages were then analyzed with Student's T-test to determine statistical significance.

Fluorophore labeled αS incorporation into protein aggregates

In order to ensure labeling does not significantly disrupt the normal behavior of the αS, we measured the incorporation of double labeled αS into protein aggregates. 70 μM unlabeled αS in 20mM Tris 140mM NaCl pH 3.0 was put at 37°C for 4 days, which induces αS aggregation to amyloid fibrils. 3.5 μM αS double cysteine mutants labeled with Texas Red (all five mutants used in Figure 2) was also added to the aggregation reactions. The Texas Red absorbance in the supernatant was measured before and after aggregation had occurred, and this was used to quantify the incorporation of the Texas Red-labeled αS into the aggregates (which spin out in the pellet after centrifugation for 10 minutes at 13.2K rpm). On average, 45% ± 12% of the Texas Red-labeled αS was incorporated into the αS aggregates at this time point, representative of the total amount of protein found in aggregated form.

Conformation of the N-terminus and NAC at pH 3.0

As shown in Figure S2, we observed subtle changes in the N-terminus of αS at low pH, compared to the collapse observed in the C-terminus. For constructs labeled at 54-72 and 72-92, the increase in ET_{eff} observed at low pH was a reproducible effect. However, the magnitude of the change in both cases (<0.1 ET_{eff} units) is small. It is possible the general compaction observed in the C-terminal region of αS propagates through the regions probed by these constructs as well (extending from position 54 to position 92). For constructs 54-72, 72-92, and 33-72, the width of the distribution is significantly increased at low pH, as was observed in the C-terminal region (Figure 2). This suggests that at low pH, chain dynamics throughout the protein may have slowed considerably (see main text for discussion). For αS T33C-T72C, we reproducibly observed a dramatic widening of the histogram at low pH. At least two possible scenarios can account for this observation. One is that the same mechanisms leading to peak broadening in other regions of the protein, which we believe is restricted chain motion at low pH, contribute more dramatically in this region. A second possibility is that two subpopulations are sampled in this region at low pH, which manifests as a main peak with a significant shoulder. The presence of a second, lower ET_{eff} population would suggest the formation of some extended structure in this region of αS at low pH. However, our data for other mutants which span this region (54-72 and 9-54) is not consistent with the population of significant extended structure, so we conclude that the widening observed in 33-72 histograms at low pH is likely due to restricted chain movement.

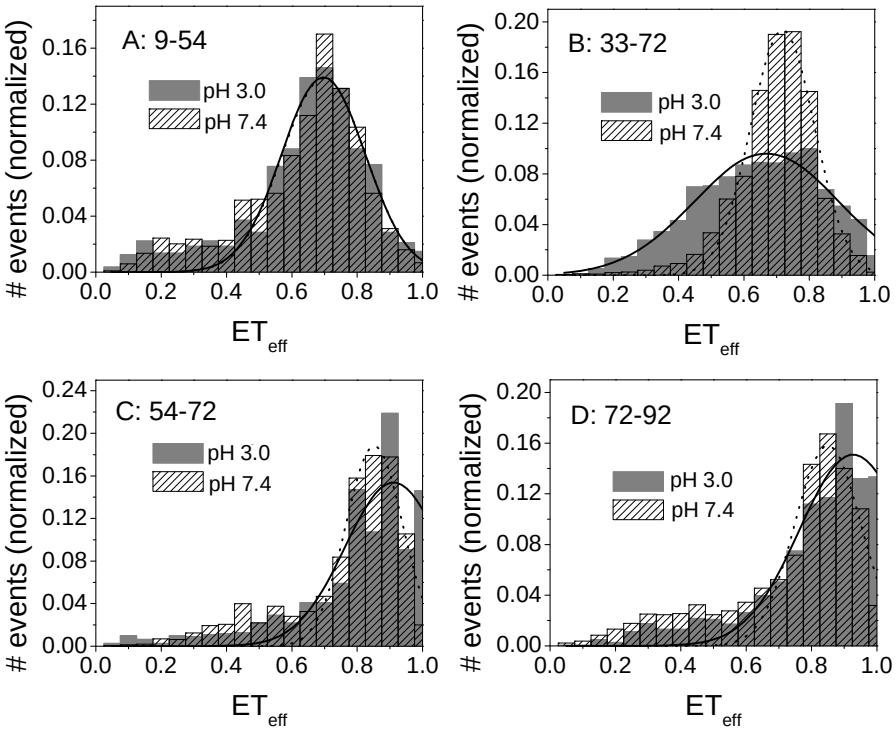

Figure S2. Low pH does not cause significant conformational changes in the N-terminal or NAC regions of αS as seen by overlap of the ET_{eff} histograms at pH 7.4 and 3.0. A-D: ET_{eff} histograms of αS at pH 7.4 and 3.0, with the labeling positions indicated in each panel. pH 7.4 distributions are shown in black hatch marks, and pH 3.0 distributions are shown as solid gray. Lines are Gaussian fits to each distribution.

Effect of DDC binding on αS conformational

Based on far-UV and FTIR measurements, the pesticide diethyldithiocarbamate (DDC) has been suggested to induce partial folding in αS by stabilizing transient hydrophobic interaction in the protein (10, 11). We investigated the conformational state of αS with DDC in order to determine if DDC causes the protein to populate a conformational state similar to the low pH state. We confirmed DDC binding to αS using quenching of intrinsic tyrosine fluorescence (10, 12); however, we were unable to observe the CD changes previously observed for αS after incubation with DDC. In our hands, DDC incubation at both room temperature and 37°C for 1-3 hours did not cause a change in αS CD spectra.

We also observed that the pesticide DDC does not induce C-terminal collapse in αS similar to the low pH state or significant conformational changes in any other region of αS we measured (Figure S3). While we observed small shifts between ET_{eff} distributions of αS in buffer in the absence or presence of DDC, it is clear DDC does not induce substantial conformational changes in αS or dramatic C-terminal compaction as low pH does. Incubation with DDC overnight with αS at either pH 7.4 or pH 3.0 also did not lead to measurable conformational differences. For the smFRET measurements, 100 μM DDC was used, over 7 orders of magnitude greater than the 90 pM αS.

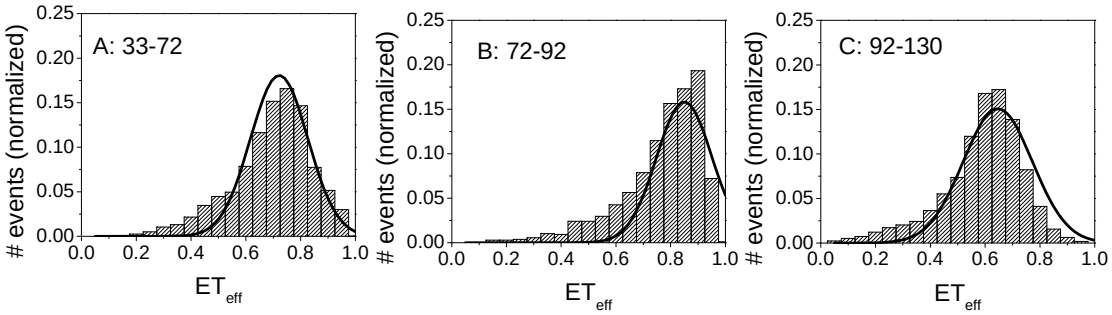

Figure S3. The pesticide DDC does not induce C-terminal collapse or other significant conformational changes in αS. Each panel shows the indicated αS mutant with 100 μM DDC. The black lines are Gaussian fits to the same αS construct in pH 7 buffer.

It is unclear what effect DDC has on αS structure and how this accelerates aggregation. It is certainly possible that DDC induces structural changes that are not accessible to our methodologies. On the other hand, given that DDC has partial negative charge in the dithio group, it is possible this molecule also acts a general charge screening compound to accelerate aggregation. Another possibility is that the site of DDC-mediated aggregation acceleration is not monomeric αS; DDC could bind and stabilize oligomeric structures, thus shifting αS equilibrium towards aggregation. The change reported in previous CD measurements of αS with DDC (CD measured at 35μM αS, over 6 orders of magnitude greater than the 90pM used for our smFRET experiments) could be due to a small percentage of protein aggregates bound by DDC (11).

GdnHCl (M)	σ
0	0.22
0.5	0.2
1.0	0.17
1.5	0.19
2.0	0.17
3.0	0.26

Table S2. Widths of Gaussian fits to histograms of GdnHCl denaturation data of contruct 72-130 (peak position shown in Figure 4 in the main text). Representative FWHM (σ) from Gaussian fits of the ET_{eff} distribution at each concentration of GdnHCl are given. As described in main text, width remained constant (average value= 0.19) for GdnHCl concentrations less than 3M.

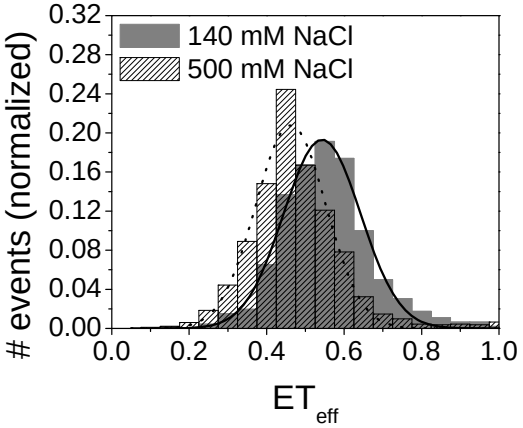

Figure S4. Charge screening with NaCl does not induce C-terminal collapse. Gray histogram is αS construct 72-130 in pH 7.4 buffer with 140 mM NaCl, black diagonal histogram is pH 7.4 with 500 mM NaCl. No further expansion was observed with 1M NaCl.

References

1. Lemke, E. A., Y. Gambin, V. Vandelinder, E. M. Brustad, H. W. Liu, P. G. Schultz, A. Groisman, and A. A. Deniz. 2009. Microfluidic device for single-molecule experiments with enhanced photostability. J. Am. Chem. Soc. 131:13610-13612.
2. Trexler, A. J., and E. Rhoades. 2009. Alpha-synuclein binds large unilamellar vesicles as an extended helix. Biochemistry 48:2304-2306.
3. Schuler, B., and W. A. Eaton. 2008. Protein folding studied by single-molecule FRET. Curr. Opin. Struct. Biol. 18:16-26.
4. Schuler, B., E. A. Lipman, and W. A. Eaton. 2002. Probing the free-energy surface for protein folding with single-molecule fluorescence spectroscopy. Nature 419:743-747.
5. Ferreon, A. C., C. R. Moran, J. C. Ferreon, and A. A. Deniz. 2010. Alteration of the alpha-synuclein folding landscape by a mutation related to Parkinson's disease. Angew Chem Int Ed Engl 49:3469-3472.
6. Lakowicz, J. 2006. Principles of Fluorescence Spectroscopy. Springer, New York, NY.
7. McCarney, E. R., J. H. Werner, S. L. Bernstein, I. Ruczinski, D. E. Makarov, P. M. Goodwin, and K. W. Plaxco. 2005. Site-specific dimensions across a highly denatured protein; a single molecule study. J Mol Biol 352:672-682.
8. Middleton, E. R., and E. Rhoades. 2010. Effects of curvature and composition on α–Synuclein binding to lipid vesicles. submitted to Biophys. J.
9. Rhoades, E., T. F. Ramlall, W. W. Webb, and D. Eliezer. 2006. Quantification of alpha-synuclein binding to lipid vesicles using fluorescence correlation spectroscopy. Biophys. J. 90:4692-4700.
10. Uversky, V. N., J. Li, K. Bower, and A. L. Fink. 2002. Synergistic effects of pesticides and metals on the fibrillation of alpha-synuclein: implications for Parkinson's disease. Neurotoxicology 23:527-536.
11. Uversky, V. N., J. Li, and A. L. Fink. 2001. Pesticides directly accelerate the rate of alpha-synuclein fibril formation: a possible factor in Parkinson's disease. FEBS Lett. 500:105-108.
12. Li, J., V. N. Uversky, and A. L. Fink. 2002. Conformational behavior of human alpha-synuclein is modulated by familial Parkinson's disease point mutations A30P and A53T. Neurotoxicology 23:553-567.